








Non-Markovian skin effect

Po-Chen Kuo ^{1,2,3,4,*} Shen-Liang Yang ^{1,2,*} Neill Lambert ^{3,4,†} Jhen-Dong Lin ^{1,2}
 Yi-Te Huang ^{1,2,3,4} Franco Nori ^{3,4,5} and Yueh-Nan Chen ^{1,2,6,‡}

¹Department of Physics, National Cheng Kung University, Tainan 701, Taiwan

²Center for Quantum Frontiers of Research and Technology, NCKU, Tainan 701, Taiwan

³Theoretical Quantum Physics Laboratory, Cluster for Pioneering Research, RIKEN, Wakoshi, Saitama 351-0198, Japan

⁴Center for Quantum Computing, RIKEN, Wakoshi, Saitama 351-0198, Japan

⁵Quantum Research Institute, The University of Michigan, Ann Arbor, Michigan 48109-1040, USA

⁶Physics Division, National Center for Theoretical Sciences, Taipei 106319, Taiwan



(Received 22 March 2024; accepted 12 February 2025; published 12 March 2025)

The Liouvillian skin effect and the non-Hermitian skin effect have both been used to explain the localization of eigenmodes near system boundaries, though the former is arguably more accurate in some regimes due to its incorporation of quantum jumps. However, these frameworks predominantly focus on weak Markovian interactions, neglecting the potentially crucial role of memory effects. To address this, we investigate, utilizing the powerful hierarchical equations of motion method, how a non-Markovian environment can modify the Liouvillian skin effect. We demonstrate that a non-Markovian environment can induce a “thick skin effect,” where the skin mode broadens and shifts into the bulk. We further identify that the skin-mode quantum coherence can only be generated when the coupling contains counter-rotating terms, leading to the coherence delocalization and oscillatory relaxation with a characteristic linear scaling with system size. Remarkably, both the skin-mode and steady-state coherence exhibit resistance to decoherence from additional environmental noise. These findings highlight the profound impact of system-bath correlations on relaxation and localization, revealing unique phenomena beyond conventional Markovian approximations.

DOI: [10.1103/PhysRevResearch.7.L012068](https://doi.org/10.1103/PhysRevResearch.7.L012068)

Introduction—The skin effect, where wavefunctions localize at system boundaries under specific conditions, is crucial in condensed matter physics [1–3] and quantum optics [4]. Extensive research has explored the non-Hermitian skin effect [5–7], where nontrivial skin-topological modes arise from gain and loss interplay [8], impacting topological classification [9–13], dynamical phase transitions [14,15], and quantum state engineering [16].

Recent theoretical advances have extended the skin effect concept to Lindblad master equations, termed the Liouvillian skin effect (LSE) [17–21]. This generalization emerges from the Liouville-von Neumann equation [22], governing the temporal evolution of the system density matrix $\rho_s(t)$. Current LSE investigations predominantly rely on the Born-Markov approximation [23]. The LSE, incorporating quantum jumps from system-environment interactions, offers a more accurate description of open quantum systems [24–27]. This phenomenon manifests as anomalous localization of eigenmodes

at system boundaries, driven by nonreciprocal dissipation, potentially extending relaxation time τ without closing the Liouvillian gap Δ [17,21].

While Markovian approaches have provided valuable insights, many realistic scenarios involve strong system-environment interactions or long-lasting correlations, leading to non-Markovian effects with profound implications [22,28,29]. These effects enhance quantum coherence [30], protect quantum information [31], enable quantum metrology [32,33], and modify quantum transport [34–38]. They can also improve quantum device performance [39] and influence chemical reaction kinetics [40].

An intriguing aspect to consider is how non-Markovian dynamics impacts the LSE, as current studies primarily rely on the Born-Markov approximation. This assumption breaks down for ultrastrong system-bath coupling [41–45] and in many realistic settings involving complex environments with memory effects [46–48]. Therefore, a comprehensive understanding of the skin effect in the non-Markovian regime is needed. A central question is whether the established relationship between relaxation time τ and system size N , expressed in terms of the localization length ξ , remains valid [17] under non-Markovian conditions:

$$\tau \stackrel{?}{\sim} \frac{1}{\Delta} + \frac{N}{\Delta\xi}. \quad (1)$$

In this work, we employ the Hierarchical equations of motion (HEOM) approach, offering nonperturbative [38,49,50]

*These authors contributed equally to this work.

†Contact author: nwlambert@gmail.com

‡Contact author: yuehnan@mail.ncku.edu.tw

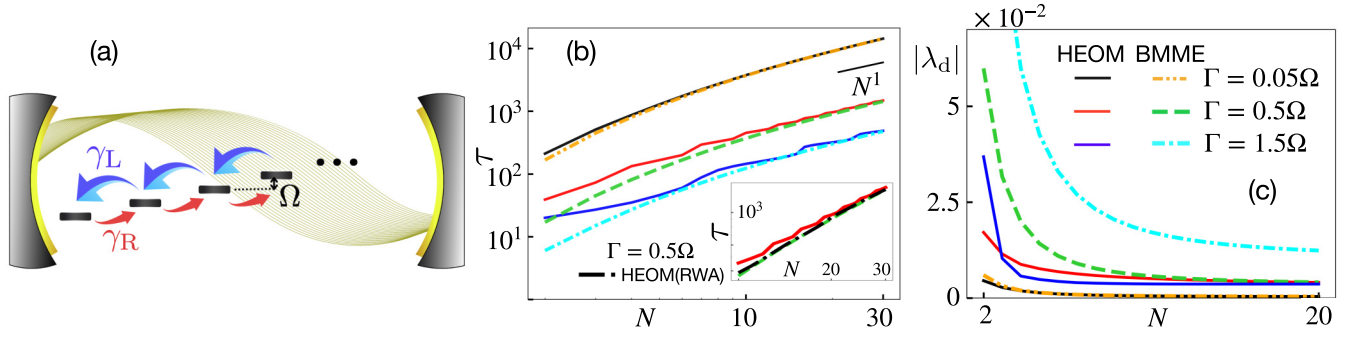


FIG. 1. (a) Schematic of an N -site 1D chain with detuning Ω and nonreciprocal hopping ($\gamma_L \neq \gamma_R$) coupled to a bosonic environment. (b) Relaxation time τ vs N in Markovian (dashed) and non-Markovian (solid) regimes for $\Gamma = 0.05, 0.5, 1.5\Omega$. Black line shows N^1 scaling. Inset: τ vs N for BMME, HEOM, and RWA-HEOM at $\Gamma = 0.5\Omega$. (c) Dominant eigenvalue magnitude $|\lambda_d|$ vs N for different Γ . Parameters: $T = 1.44\Omega$, $W = \Omega$, $l_{\max} = 20$, $m_{\max} = 4$ (8 for $\Gamma = 1.5\Omega$).

and non-Markovian characterization [51,52] of environmental effects, to investigate the non-Markovian skin effect. Our abstract model reveals features including (i) a “thick skin” effect with delocalized steady-state population at the boundary, (ii) emergence of persistent cross-site quantum coherence in skin-localized modes under decoherence noise, and (iii) secondary skin-localized modes modulating oscillatory relaxation dynamics.

We here consider a single particle in an N -site 1D lattice coupled to a bosonic bath as shown in Fig. 1. The system Hamiltonian is given by (with $\hbar = 1$ throughout) $H_s = \sum_{n=1}^N \omega_n d_n^\dagger d_n$, where d_n (d_n^\dagger) corresponds to the creation (annihilation) operator of the particle within the n th site. We assume identical energy detuning $\Omega = \omega_n - \omega_{n-1}$ between adjacent sites, with the particle initially in the highest energy state. To induce the skin effect, we introduce thermally induced nonreciprocal hopping via a bosonic bath with correlation function

$$C(\tau) = \frac{1}{2\pi} \int_0^\infty d\omega J(\omega) \{n^{\text{eq}}(\omega) e^{i\omega\tau} + [n^{\text{eq}}(\omega) + 1] e^{-i\omega\tau}\}, \quad (2)$$

where $n^{\text{eq}}(\omega) = \{\exp[\omega/k_B T] - 1\}^{-1}$, representing the Bose-Einstein distribution with k_B as the Boltzmann constant and T as the temperature. We assume a Drude-Lorentz spectral density $J(\omega) = 4\Gamma W\omega/(\omega^2 + W^2)$, where Γ represents the coupling strength between the system and the bosonic reservoir with bandwidth W . We also explore the non-Markovian skin effect under other choices of bath spectral densities to understand the role of the environment’s structure [23]. Assuming closely spaced sites enabling collective coupling to a common bath [53,54], the system-bath interaction is given by $H_I = V_{\text{ob}} \sum_k g_k (a_k + a_k^\dagger)$, where system interaction operator $V_{\text{ob}} = \sum_n (d_n^\dagger d_{n+1} + d_{n+1}^\dagger d_n)$ mediates nearest-neighbor hopping. For distant sites coupled to independent baths, $H_I = \sum_n V_{\text{ob},n} \sum_k g_{n,k} (a_{n,k} + a_{n,k}^\dagger)$ with $V_{\text{ob},n} = d_n^\dagger d_{n+1} + d_{n+1}^\dagger d_n$ [55]. While both cases can exhibit the LSE, we focus on the richer collective coupling scenario, with results for the noncollective case presented in the Supplemental Material [23].

For the Markovian case, nonreciprocal hopping can be determined by the asymmetric dissipation rate for left and right hopping, $\gamma_L = J(\Omega)[n^{\text{eq}}(\Omega) + 1]m$ and $\gamma_R =$

$J(\Omega)n^{\text{eq}}(\Omega)$, respectively, encoded in the Lindblad operators $L_L = \sqrt{\gamma_L} \sum_{n=1}^{N-1} d_n^\dagger d_{n+1}$ and $L_R = \sqrt{\gamma_R} \sum_{n=1}^{N-1} d_{n+1}^\dagger d_n$, according to BMME in Eq. (A23) [23]. This thermally induced asymmetry allows for flexible control of the γ_L/γ_R ratio by adjusting the temperature. This asymmetric thermally induced hopping is realizable in various systems, including photonic topological lattices [56,57], ultracold atoms in an optical lattice driven by laser-assisted hopping with spontaneous emission [58–60], trapped-ion systems where lasers couple internal states to external motional sideband states [61–63], and 1D quantum dots where transport electrons couple to photon bath [64–68]. For simplicity, we set $\gamma_L/\gamma_R \approx 2$ throughout.

In the non-Markovian case, nonreciprocal hopping necessitates going beyond the Born-Markov and secular approximations, incorporating non-Markovian and nonperturbative effects [51,69]. This is achieved using the interaction operator V_{ob} within the HEOM generator [38,49,70] in Eq. (3), as detailed in the following section.

HEOM-derived skin effect—To incorporate the non-Markovian and nonperturbative effects we employ the HEOM method, which relies on a Liouvillian superoperator operating on a system’s (s) space expanded by auxiliary density operators (ADOs). These ADOs encode environmental influence and memory effects arising from system-bath interactions [71]. Each ADO relates to an exponential term in the decomposition of the correlation function $C(\tau) = \sum_{u=\mathbb{R},\mathbb{I}} (\delta_{u,\mathbb{R}} + i\delta_{u,\mathbb{I}}) C^u(\tau)$, where \mathbb{R} and \mathbb{I} , respectively, denote the real and imaginary parts of $C^u(\tau) = \sum_l^{\text{max}} \xi_l^u \exp(-\chi_l^u \tau)$ [23]. The HEOM generator $\hat{\mathcal{L}}_H$, operating on the combined system-ADO space $\rho_{s+\text{ADO}}(t)$, characterizes the dynamics as follows [38,72–74]:

$$\frac{\partial}{\partial t} \text{vec}[\rho_{s+\text{ADO}}(t)] = \hat{\mathcal{L}}_H \text{vec}[\rho_{s+\text{ADO}}(t)], \quad (3)$$

where $\text{vec}[\cdot]$ denotes vectorization for eigensolving. This HEOM generator encodes system-bath interactions through V_{ob} . Subsequently, the right and left eigenmodes of the $\hat{\mathcal{L}}_H$ are defined by [74]

$$\hat{\mathcal{L}}_H \rho_i^R = \lambda_i \rho_i^R, \quad \rho_j^L \hat{\mathcal{L}}_H = \lambda_j \rho_j^L, \quad (4)$$

where $\lambda_{i(j)}$ is the i th (j th) eigenvalue with the corresponding right ρ_i^R (left ρ_j^L) eigenmode. The HEOM-space inner product of two ADO vectors is defined as $(\rho_a^u | \rho_b^v) =$

$\sum_k \rho_a^{v\dagger}[k] \cdot \rho_b^v[k]$, where k indexes elements in each eigenmode. The trace norm of an ADO is then $\|\rho_i^v\| = (\sum_k \rho_i^{v\dagger}[k] \rho_i^v[k])^{1/2}$. The first right eigenmode ρ_0^R with $\lambda_0 = 0$ corresponds to the stationary state $\hat{\rho}_{ss} = \rho_0^R / \text{Tr}(\rho_{0,s}^R)$, ensuring probability preservation. Here, the subscript s in $\rho_{0,s}^R$ denotes the system reduced density matrix within the ADOs. The HEOM dynamics can be decomposed into the right eigenmodes [23]:

$$\text{vec}[\rho_{s+\text{ADO}}(t)] = \hat{\rho}_{ss} + \sum_{i=1}^{N_{\text{tot}}} c_i e^{\lambda_i t} \hat{\rho}_i^R, \quad (5)$$

where $N_{\text{tot}} = N_s^2 \times N_{\text{ADO}}$, with N_s and N_{ADO} denoting the dimension of H_s and the number of ADO, respectively. Here, $c_i = \|\rho_i^L\| \|\rho_i^R\| \langle \hat{\rho}_i^L | \text{vec}[\hat{\rho}_{\text{ini}}] \rangle$, where $\hat{\rho}_{\text{ini}}$ represents an arbitrary initial state. We assume that $\hat{\rho}_{\text{ini},s} = |N\rangle\langle N|$ with no initial system-bath correlation. Following Ref. [17], the long-time system dynamics are governed by the steady-state eigenmode $\hat{\rho}_{ss}$ and the dominant eigenmode $\hat{\rho}_d$ with eigenvalue λ_d . The relaxation time τ , defined as the time at which the contribution of $\hat{\rho}_d$ surpasses all other eigenmodes, is when $|c_d(\tau)| = e^{-1}$, where $c_d(\tau) = c_d \exp(-\tau \lambda_d)$. While $\hat{\rho}_d$ is the dominant mode, virtual processes arising from counter-rotating terms can introduce secondary skin modes that also influence relaxation, unlike in the Markovian regime. Furthermore, the HEOM-derived coefficient c_d exhibits an N dependence, following the relation $\|\rho_i^L\| \|\rho_i^R\| \sim e^{O(N/\xi_H)}$, where ξ_H is the HEOM-derived localization length. The HEOM-derived relaxation time is thus

$$\tau \sim \frac{1}{\lambda_d} + \frac{N}{\lambda_d \xi_H}. \quad (6)$$

We aim to demonstrate the hallmark of non-Markovian LSE by examining the relaxation time τ and the dominant eigenvalue λ_d , which corresponds to the Liouvillian gap in the Markovian limit.

Relaxation time—Both the Markovian (BMME) and non-Markovian (HEOM) approaches are employed here. We observe two key trends as shown in Fig. 1. In the strong-coupling regime ($\Gamma \geq 0.5\Omega$), there is a notable difference between the results of BMME and HEOM. The HEOM yields a slower relaxation (larger τ) corresponding to a larger dominant eigenvalue λ_d [Fig. 1(b)] compared that of the BMME.

The impact of the non-Markovian effect is revealed by comparing HEOM and BMME results, particularly in the relaxation-determining parameter λ_d . For instance, when $\Gamma = 0.05\Omega$, the values of λ_d are consistent between BMME and HEOM under the Markovian condition. In contrast, when $\Gamma > 0.5\Omega$, the deviation in λ_d is obvious, indicating a transition to the non-Markovian regime.

Moreover, as N increases, both approaches exhibit a direct linear relationship in τ , while λ_d [Fig. 1(c)] and the localization length ξ_H [Fig. 2(c)] approach constant values. This signifies that even under the non-Markovian dynamics, the LSE persists, as inferred from Eq. (6), and governs the long-time relaxation behavior at larger system sizes. Furthermore, in the strong-coupling regime, the relaxation time displays additional small oscillations. Notably, when we implement the rotating-wave approximation in HEOM (RWA-HEOM) to remove the counter-rotating terms ($d_{n+1}^\dagger d_n a_k^\dagger$ and $a_k d_n^\dagger d_{n+1}$ in

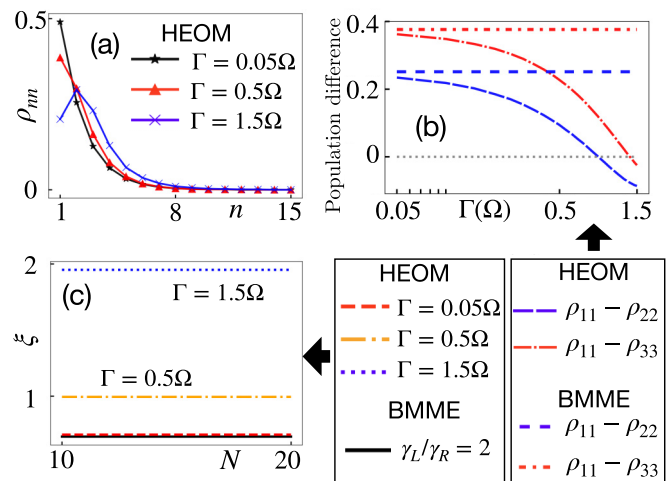


FIG. 2. (a) Site populations in $\rho_{0,s}^R$ for different Γ in the non-Markovian regime (HEOM). (b) Population differences $\rho_{11} - \rho_{22}$ (dashed) and $\rho_{11} - \rho_{33}$ (dash dotted) vs Γ for BMME and HEOM. (c) Localization length ξ of $\hat{\rho}_d$ vs N for different Γ in Markovian (BMME) and non-Markovian (HEOM) regimes. Here, $\gamma_L/\gamma_R = 2$ for BMME.

H_1), these oscillations disappear. This indicates that not every non-Markovian effect can induce the oscillations. Only the virtual processes generated by the counter-rotating terms can induce such oscillations. The connection between the oscillations and virtual processes will be further investigated later.

Thick skin effect—A key signature of the Liouvillian skin effect is eigenmode localization. We focus on the steady-state eigenmode $\rho_{0,s}^R$ to examine the localization of the site population. In weak-coupling scenarios, this population is predominantly localized at the system’s boundary. However, in the strong-coupling regime, non-Markovian dynamics can induce gradual delocalization of $\rho_{0,s}^R$, redistributing population across energy levels [Fig. 2(a)]. This redistribution stems from the enhanced system-bath interactions, facilitating energy and information exchange between the system and bath. Consequently, higher energy levels can maintain nonzero populations in the steady-state eigenmode, effectively “repopulating” levels that typically deplete in a Markovian system. When $\Gamma \approx \Omega$, the population extends to the second or third site, potentially exceeding that of the first site. While this deeper and broadening localization of the population extends further into the chain, it still adheres to LSE principles. We term this the “thick skin effect,” which cannot be captured by BMME, highlighting the inadequacy of Markovian approaches in this domain [Fig. 2(b)]. The “thick skin effect” manifests as an expansion in the localization length ξ_H for $\hat{\rho}_d$ [Fig. 2(c)]. In the non-Markovian regime, this expansion adheres to LSE behavior and remains independent of system size N , consistent with LSE phenomena.

Emergence and resilience of quantum coherence induced by the virtual process—The eigenspectrum of the HEOM generator reveals a rich structure that significantly deviates from the BMME Liouvillian, as illustrated in Fig. 3(a). The steady-state eigenmode $\hat{\rho}_{ss}$ corresponds to λ_0 , while the primary skin mode $\hat{\rho}_d$ is associated with λ_d . Notably, the HEOM approach unveils secondary skin modes $\hat{\rho}_{\text{coh}}^{(\dagger)}$ with complex eigenvalues,

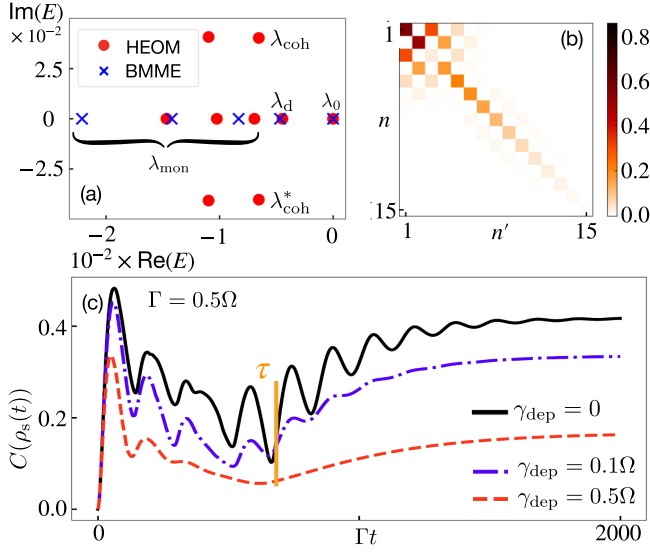


FIG. 3. (a) Eigenspectrum obtained from BMME (blue) and HEOM (red) Liouvillian superoperators. Eigenvalues λ_0 , λ_d , $\lambda_{\text{coh}}^{(\dagger)}$, and λ_{mon} correspond to $\hat{\rho}_{\text{ss}}$, $\hat{\rho}_d$, $\hat{\rho}_{\text{coh}}^{(\dagger)}$, and $\hat{\rho}_{\text{mon}}$, respectively. (b) Color plots of the reduced density matrix extracted from $\hat{\rho}_d$ for $N = 15$ obtained using HEOM. (c) Dynamics of coherence $C(\rho_s(t))$ at $\Gamma = 0.5\Omega$ under the dephasing applied to all sites with the rate γ_{dep} .

$\lambda_{\text{coh}}^{(\dagger)}$, showing oscillatory behavior. The monotonically decaying modes $\hat{\rho}_{\text{mon}}$ are represented by λ_{mon} . Crucially, both $\hat{\rho}_d$ and $\hat{\rho}_{\text{mon}}$ in HEOM exhibit eigenvalues closer to λ_0 compared to that of BMME, accounting for the extended relaxation time.

A striking feature of the HEOM-derived eigenmodes, including the skin modes, is the presence of cross-site coherence [Fig. 3(b)], while the quantum coherence between any two adjacent sites is zero. Such a coherence is absent in both BMME and RWA-HEOM approaches. This coherence, quantified by the l_1 norm $C(\rho_s(t)) = \sum_{n \neq n'} |\rho_s(t)[n, n']|$ [75], can be attributed to the virtual processes involving simultaneous creation or annihilation of two excitations. These processes underscore the importance of the counter-rotating terms when considering non-Markovian effects. The temporal evolution of the coherence induced by the virtual processes, primarily driven by $\hat{\rho}_{\text{coh}}^{(\dagger)}$, exhibits oscillatory behavior [Fig. 3(c)]. Remarkably, this cross-site coherence persists even beyond the relaxation time $t = \tau$ [Fig. 3(c), orange short vertical segment], even when strong on-site dephasing is present at every site [76,77]. This dephasing is modeled within the BMME framework (Eq. (A24) [23]) by incorporating the Lindblad dissipator $\sum_{n=1}^N \mathcal{J}(L_{\text{nos},n})$, where $L_{\text{nos},n} = \sqrt{\gamma_{\text{dep}}} d_n^\dagger d_n$. This unexpected resilience arises from the interplay between the strong system-bath interactions and the dephasing. Through the virtual processes, the total system is effectively projected into the preferred eigenstates. These processes include not only the conventional transitions to $\approx |e_n, N_{\text{ph}} + 1\rangle \pm |g_n, N_{\text{ph}}\rangle$, but also the higher-order transitions to $\approx |e_n, N_{\text{ph}}\rangle \pm |g_n, N_{\text{ph}} + 1\rangle$. Here, e_n (g_n) represents the occupied (vacant) particle state hybridized with either $N_{\text{ph}} + 1$ or N_{ph} from the bath. This hybridization maintains the coherence even in the presence of dephasing at every site [76–78]. These findings

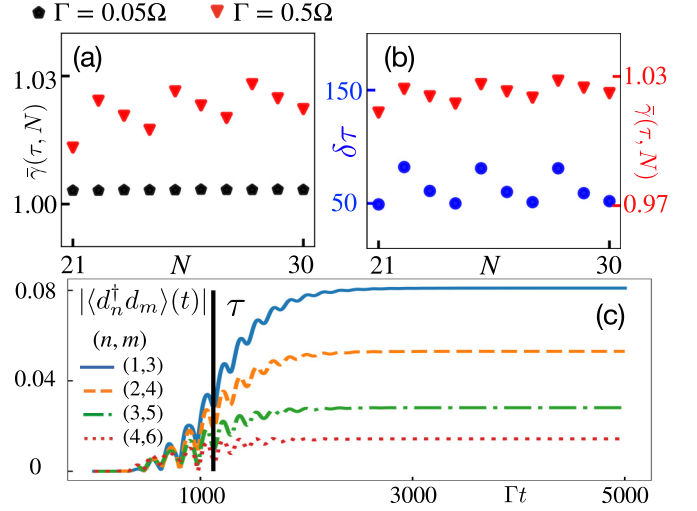


FIG. 4. (a) $\bar{\gamma}(\tau, N)$ versus N for $\Gamma = 0.05\Omega$ (black hexagons) and $\Gamma = 0.5\Omega$ (red triangles). (b) Relaxation time deviation $\delta\tau$ between HEOM and BMME approaches (blue circles, left axis), and $\bar{\gamma}(\tau, N)$ (red triangles, right axis), both as a function of N for $\Gamma = 0.5\Omega$. (c) Time evolutions of $|\langle d_n^\dagger d_m \rangle(t)|$ for different values of (n, m) .

highlight the intriguing possibilities for the decoherence resistance within the regime of the non-Markovian skin effect.

Coherence delocalization—We now stress an intriguing observation regarding the properties of the LSE in relation to τ , which exhibits a linear dependence on N . However, what makes this behavior even more interesting is the presence of distinct oscillations in τ versus N . To delve into the underlying particle transport mechanisms driving this phenomenon, we calculate the average scaled rate of particle transport up to τ along this 1D chain [79]:

$$\bar{\gamma}(\tau, N) \approx \frac{1}{\tau} \sum_{n=1}^N \int_0^\tau \gamma(t, N) dt, \quad (7)$$

where $\gamma(t, N) = \sum_{n=1}^N [\langle d_n^\dagger d_n \rangle(t) + \sum_{n \neq m} \langle d_n^\dagger d_m \rangle(t)]$. The second term in $\gamma(t, N)$ accounts for superradiant contributions arising from intersite coherence. As the coupling strength Γ approaches 0.5Ω in the non-Markovian regime, we observe the increase in $\bar{\gamma}(\tau, N)$ compared to the weak-coupling case as shown in Fig. 4(a). This enhancement solely stems from the second term in $\gamma(t, N)$ in Eq. (7), as the first term (representing individual site population) remains constant due to trace preservation [23]. The intriguing small oscillations in the non-Markovian LSE τ observed in Fig. 1 correlate with sharp changes in the $\bar{\gamma}(\tau, N)$ with respect to N . We quantify this connection by analyzing the deviation in τ obtained from HEOM compared to the BMME, i.e., $\delta\tau$. As shown in Fig. 4(b), the periodic maxima and minima of $\delta\tau$ align with the corresponding peaks and valleys in $\bar{\gamma}(\tau, N)$. This alignment between $\delta\tau$ and $\bar{\gamma}(\tau, N)$ can be understood through the analysis of the eigenmode energy spectrum [23].

Note that the dynamics of $\gamma(t, N)$ constitute an important part of $\bar{\gamma}(\tau, N)$. We observe that the $\langle d_n^\dagger d_m \rangle(t)$ term in $\gamma(t, N)$ clearly demonstrates the effect of virtual processes induced by the counter-rotating terms in the strong-coupling regime. As illustrated in Fig. 4(c), only cross-site $\langle d_n^\dagger d_m \rangle(t)$ terms

contribute significantly to $\gamma(t, N)$, such as $(n, m) = (1, 3), (2, 4)$, and even $(3, 5), (4, 6)$. This is a phenomenon analogous to the cross-site coherence, i.e., no contribution from any two adjacent sites. An intuitive picture of this effective cross-site coupling, $\langle d_n^\dagger d_m \rangle(t)$, can be conceptualized using a three-site model: A particle moving from the third site to the second site, via the conventional transition operator $d_n^\dagger d_{n+1} a_k^\dagger$, generates a boson. This boson can subsequently undergo a virtual process (higher-order transition) facilitated by the counter-rotating term $d_n^\dagger d_{n+1} a_k$, enabling the particle to further transit to the first site. This composite transition process generates the cross-site $\langle d_n^\dagger d_m \rangle(t)$ terms, thereby creating the cross-site quantum correlations.

In other words, the emergence of intersite coherence, facilitated by the non-Markovian effect with virtual process, can hinder the skin effect's tendency to localize particles at the system edge. In this sense, the intersite coherence plays a similar role to Anderson localization in the well-known competition between skin effect and Anderson localization in many-body systems. Both phenomena can impede the skin effect's localization tendency, influencing the particle transport dynamics [80].

Conclusions—Our investigation of the “non-Markovian skin effect” reveals unique signatures not captured by conventional Markovian treatments. These include thick skin

effect, persistent coherence in non-Markovian eigenmodes even under local decoherence, and coherence-delocalization effect at the relaxation time. These findings pave the way for exciting future research, such as exploring diverse systems and boundary conditions, delving into multiparticle scenarios, and investigating the impact on topological features like the winding number [5]. Such investigations hold promise for unlocking novel applications in various areas, including controlling light [81,82] and electron localization [80,83,84], manipulating directional transport phenomena [85–88], influencing critical entanglement properties [15], and enhancing the sensitivity of topological sensors [89,90].

Acknowledgments—F.N. is supported in part by Nippon Telegraph and Telephone Corporation (NTT) Research, the Japan Science and Technology Agency (JST) [via the CREST Quantum Frontiers program Grant No. 24031662, the Quantum Leap Flagship Program (Q-LEAP), and the Moonshot R&D Grant Number JPMJMS2061], and the Office of Naval Research Global (ONR) (via Grant No. N62909-23-1-2074). N.L. is supported by the RIKEN Incentive Research Program and by MEXT KAKENHI Grants No. JP24H00816 and No. JP24H00820. Y.N.C. acknowledges the support of the National Center for Theoretical Sciences and the National Science and Technology Council, Taiwan (NSTC Grant No. 113-2123-M-006-001).

-
- [1] C. H. Lee, L. Li, and J. Gong, Hybrid higher-order skin-topological modes in nonreciprocal systems, *Phys. Rev. Lett.* **123**, 016805 (2019).
- [2] N. Okuma and M. Sato, Non-Hermitian skin effects in Hermitian correlated or disordered systems: Quantities sensitive or insensitive to boundary effects and pseudo-quantum-number, *Phys. Rev. Lett.* **126**, 176601 (2021).
- [3] R. Lin, T. Tai, L. Li, and C. H. Lee, Topological non-Hermitian skin effect, *Front. Phys.* **18**, 53605 (2023).
- [4] L. Li, C. H. Lee, and J. Gong, Topological switch for non-Hermitian skin effect in cold-atom systems with loss, *Phys. Rev. Lett.* **124**, 250402 (2020).
- [5] L. Zhang, Y. Yang, Y. Ge, Y.-J. Guan, Q. Chen, Q. Yan, F. Chen, R. Xi, Y. Li, D. Jia, S.-Q. Yuan, H.-X. Sun, H. Chen, and B. Zhang, Acoustic non-Hermitian skin effect from twisted winding topology, *Nat. Commun.* **12**, 6297 (2021).
- [6] X.-Q. Sun, P. Zhu, and T. L. Hughes, Geometric response and disclination-induced skin effects in non-Hermitian systems, *Phys. Rev. Lett.* **127**, 066401 (2021).
- [7] X. Zhang, Y. Tian, J.-H. Jiang, M.-H. Lu, and Y.-F. Chen, Observation of higher-order non-Hermitian skin effect, *Nat. Commun.* **12**, 5377 (2021).
- [8] Y. Li, C. Liang, C. Wang, C. Lu, and Y.-C. Liu, Gain-loss-induced hybrid skin-topological effect, *Phys. Rev. Lett.* **128**, 223903 (2022).
- [9] T. Liu, J. J. He, T. Yoshida, Z.-L. Xiang, and F. Nori, Non-Hermitian topological Mott insulators in one-dimensional fermionic superlattices, *Phys. Rev. B* **102**, 235151 (2020).
- [10] T. Hofmann, T. Helbig, F. Schindler, N. Salgo, M. Brzezińska, M. Greiter, T. Kiessling, D. Wolf, A. Vollhardt, A. Kabašić, C. H. Lee, A. Bilušić, R. Thomale, and T. Neupert, Reciprocal skin effect and its realization in a topoelectrical circuit, *Phys. Rev. Res.* **2**, 023265 (2020).
- [11] L. S. Palacios, S. Tchoumakov, M. Guix, I. Pagonabarraga, S. Sánchez, and A. G. Grushin, Guided accumulation of active particles by topological design of a second-order skin effect, *Nat. Commun.* **12**, 4691 (2021).
- [12] Y. O. Nakai, N. Okuma, D. Nakamura, K. Shimomura, and M. Sato, Topological enhancement of non-normality in non-Hermitian skin effects, *Phys. Rev. B* **109**, 144203 (2024).
- [13] C. R. Leefmans, M. Parto, J. Williams, G. H. Y. Li, A. Dutt, F. Nori, and A. Marandi, Topological temporally mode-locked laser, *Nat. Phys.* **20**, 852 (2024).
- [14] K.-M. Kim and M. J. Park, Disorder-driven phase transition in the second-order non-Hermitian skin effect, *Phys. Rev. B* **104**, L121101 (2021).
- [15] K. Kawabata, T. Numasawa, and S. Ryu, Entanglement phase transition induced by the non-Hermitian skin effect, *Phys. Rev. X* **13**, 021007 (2023).
- [16] F. Song, S. Yao, and Z. Wang, Non-Hermitian skin effect and chiral damping in open quantum systems, *Phys. Rev. Lett.* **123**, 170401 (2019).
- [17] T. Haga, M. Nakagawa, R. Hamazaki, and M. Ueda, Liouvillian skin effect: Slowing down of relaxation processes without gap closing, *Phys. Rev. Lett.* **127**, 070402 (2021).
- [18] F. Yang, Q.-D. Jiang, and E. J. Bergholtz, Liouvillian skin effect in an exactly solvable model, *Phys. Rev. Res.* **4**, 023160 (2022).
- [19] S. Hamanaka, K. Yamamoto, and T. Yoshida, Interaction-induced Liouvillian skin effect in a fermionic chain with a two-body loss, *Phys. Rev. B* **108**, 155114 (2023).
- [20] G. Lee, A. McDonald, and A. Clerk, Anomalously large relaxation times in dissipative lattice models beyond the

- non-Hermitian skin effect, *Phys. Rev. B* **108**, 064311 (2023).
- [21] Z. Wang, Y. Lu, Y. Peng, R. Qi, Y. Wang, and J. Jie, Accelerating relaxation dynamics in open quantum systems with Liouvillian skin effect, *Phys. Rev. B* **108**, 054313 (2023).
- [22] H.-P. Breuer, E.-M. Laine, and J. Piilo, Measure for the degree of non-Markovian behavior of quantum processes in open systems, *Phys. Rev. Lett.* **103**, 210401 (2009).
- [23] See Supplemental Material at <http://link.aps.org/supplemental/10.1103/PhysRevResearch.7.L012068> for details on the non-Markovian skin effect.
- [24] F. Minganti, A. Biella, N. Bartolo, and C. Ciuti, Spectral theory of Liouvillians for dissipative phase transitions, *Phys. Rev. A* **98**, 042118 (2018).
- [25] F. Minganti, A. Miranowicz, R. W. Chhajlany, and F. Nori, Quantum exceptional points of non-Hermitian Hamiltonians and Liouvillians: The effects of quantum jumps, *Phys. Rev. A* **100**, 062131 (2019).
- [26] P.-C. Kuo, N. Lambert, A. Miranowicz, H.-B. Chen, G.-Y. Chen, Y.-N. Chen, and F. Nori, Collectively induced exceptional points of quantum emitters coupled to nanoparticle surface plasmons, *Phys. Rev. A* **101**, 013814 (2020).
- [27] F. Minganti, A. Miranowicz, R. W. Chhajlany, I. I. Arkhipov, and F. Nori, Hybrid-Liouvillian formalism connecting exceptional points of non-Hermitian Hamiltonians and Liouvillians via postselection of quantum trajectories, *Phys. Rev. A* **101**, 062112 (2020).
- [28] B.-H. Liu, L. Li, Y.-F. Huang, C.-F. Li, G.-C. Guo, E.-M. Laine, H.-P. Breuer, and J. Piilo, Experimental control of the transition from Markovian to non-Markovian dynamics of open quantum systems, *Nat. Phys.* **7**, 931 (2011).
- [29] D. Gribben, A. Strathearn, G. E. Fux, P. Kirton, and B. W. Lovett, Using the environment to understand non-Markovian open quantum systems, *Quantum* **6**, 847 (2022).
- [30] B. Wang, Z.-Y. Xu, Z.-Q. Chen, and M. Feng, Non-Markovian effect on the quantum discord, *Phys. Rev. A* **81**, 014101 (2010).
- [31] H.-P. Breuer, E.-M. Laine, J. Piilo, and B. Vacchini, Colloquium: Non-Markovian dynamics in open quantum systems, *Rev. Mod. Phys.* **88**, 021002 (2016).
- [32] A. W. Chin, S. F. Huelga, and M. B. Plenio, Quantum metrology in non-Markovian environments, *Phys. Rev. Lett.* **109**, 233601 (2012).
- [33] N. Mirkin, M. Larocca, and D. Wisniacki, Quantum metrology in a non-Markovian quantum evolution, *Phys. Rev. A* **102**, 022618 (2020).
- [34] C. Flindt, T. Novotný, A. Braggio, M. Sassetti, and A.-P. Jauho, Counting statistics of non-Markovian quantum stochastic processes, *Phys. Rev. Lett.* **100**, 150601 (2008).
- [35] X. Zheng, J. Luo, J. Jin, and Y. Yan, Complex non-Markovian effect on time-dependent quantum transport, *J. Chem. Phys.* **130**, 124508 (2009).
- [36] Y.-N. Chen, G.-Y. Chen, Y.-Y. Liao, N. Lambert, and F. Nori, Detecting non-Markovian plasmonic band gaps in quantum dots using electron transport, *Phys. Rev. B* **79**, 245312 (2009).
- [37] S. V. Moreira, B. Marques, R. R. Paiva, L. S. Cruz, D. O. Soares-Pinto, and F. L. Semião, Enhancing quantum transport efficiency by tuning non-Markovian dephasing, *Phys. Rev. A* **101**, 012123 (2020).
- [38] Y.-T. Huang, P.-C. Kuo, N. Lambert, M. Cirio, S. Cross, S.-L. Yang, F. Nori, and Y.-N. Chen, An efficient Julia framework for hierarchical equations of motion in open quantum systems, *Commun. Phys.* **6**, 313 (2023).
- [39] G. A. L. White, F. A. Pollock, L. C. L. Hollenberg, K. Modi, and C. D. Hill, Non-Markovian quantum process tomography, *PRX Quantum* **3**, 020344 (2022).
- [40] T. Guérin, O. Bénichou, and R. Voituriez, Non-Markovian polymer reaction kinetics, *Nat. Chem.* **4**, 568 (2012).
- [41] M. Geiser, F. Castellano, G. Scalari, M. Beck, L. Nevou, and J. Faist, Ultrastrong coupling regime and plasmon polaritons in parabolic semiconductor quantum wells, *Phys. Rev. Lett.* **108**, 106402 (2012).
- [42] R. Stassi, A. Ridolfo, O. Di Stefano, M. J. Hartmann, and S. Savasta, Spontaneous conversion from virtual to real photons in the ultrastrong-coupling regime, *Phys. Rev. Lett.* **110**, 243601 (2013).
- [43] G.-T. Chen, P.-C. Kuo, H.-Y. Ku, G.-Y. Chen, and Y.-N. Chen, Probing higher-order transitions through scattering of microwave photons in the ultrastrong-coupling regime of circuit QED, *Phys. Rev. A* **98**, 043803 (2018).
- [44] A. F. Kockum, A. Miranowicz, S. De Liberato, S. Savasta, and F. Nori, Ultrastrong coupling between light and matter, *Nat. Rev. Phys.* **1**, 19 (2019).
- [45] N. Lambert, S. Ahmed, M. Cirio, and F. Nori, Modelling the ultra-strongly coupled spin-Boson model with unphysical modes, *Nat. Commun.* **10**, 3721 (2019).
- [46] I. de Vega and D. Alonso, Dynamics of non-Markovian open quantum systems, *Rev. Mod. Phys.* **89**, 015001 (2017).
- [47] G. Andersson, B. Suri, L. Guo, T. Aref, and P. Delsing, Non-exponential decay of a giant artificial atom, *Nat. Phys.* **15**, 1123 (2019).
- [48] P.-C. Kuo, J.-D. Lin, Y.-C. Huang, and Y.-N. Chen, Controlling periodic Fano resonances of quantum acoustic waves with a giant atom coupled to a microwave waveguide, *Opt. Express* **31**, 42285 (2023).
- [49] Z. H. Li, N. H. Tong, X. Zheng, D. Hou, J. H. Wei, J. Hu, and Y. J. Yan, Hierarchical Liouville-space approach for accurate and universal characterization of quantum impurity systems, *Phys. Rev. Lett.* **109**, 266403 (2012).
- [50] N. Lambert, T. Raheja, S. Cross, P. Menczel, S. Ahmed, A. Pitchford, D. Burgarth, and F. Nori, QuTiP-BoFiN: A bosonic and fermionic numerical hierarchical-equations-of-motion library with applications in light-harvesting, quantum control, and single-molecule electronics, *Phys. Rev. Res.* **5**, 013181 (2023).
- [51] A. Kato and Y. Tanimura, Quantum heat current under non-perturbative and non-Markovian conditions: Applications to heat machines, *J. Chem. Phys.* **145**, 224105 (2016).
- [52] Y. Tanimura, Numerically “exact” approach to open quantum dynamics: The hierarchical equations of motion (HEOM), *J. Chem. Phys.* **153**, 020901 (2020).
- [53] T. Ikeda and Y. Tanimura, Probing photoisomerization processes by means of multi-dimensional electronic spectroscopy: The multi-state quantum hierarchical Fokker-Planck equation approach, *J. Chem. Phys.* **147**, 014102 (2017).
- [54] M. Cainelli, R. Borrelli, and Y. Tanimura, Effect of mixed Frenkel and charge transfer states in time-gated fluorescence spectra of perylene bisimides H-aggregates: Hierarchical equations of motion approach, *J. Chem. Phys.* **157**, 084103 (2022).
- [55] K. Nakamura and Y. Tanimura, Optical response of laser-driven charge-transfer complex described by Holstein–Hubbard model

- coupled to heat baths: Hierarchical equations of motion approach, *J. Chem. Phys.* **155**, 064106 (2021).
- [56] C. Leefmans, A. Dutt, J. Williams, L. Yuan, M. Parto, F. Nori, S. Fan, and A. Marandi, Topological dissipation in a time-multiplexed photonic resonator network, *Nat. Phys.* **18**, 442 (2022).
- [57] M. Parto, C. Leefmans, J. Williams, F. Nori, and A. Marandi, Non-Abelian effects in dissipative photonic topological lattices, *Nat. Commun.* **14**, 1440 (2023).
- [58] M. Aidelsburger, M. Atala, M. Lohse, J. T. Barreiro, B. Paredes, and I. Bloch, Realization of the Hofstadter Hamiltonian with ultracold atoms in optical lattices, *Phys. Rev. Lett.* **111**, 185301 (2013).
- [59] H. Miyake, G. A. Siviloglou, C. J. Kennedy, W. C. Burton, and W. Ketterle, Realizing the Harper Hamiltonian with laser-assisted tunneling in optical lattices, *Phys. Rev. Lett.* **111**, 185302 (2013).
- [60] Z.-C. Xiang, K. Huang, Y.-R. Zhang, T. Liu, Y.-H. Shi, C.-L. Deng, T. Liu, H. Li, G.-H. Liang, Z.-Y. Mei, H. Yu, G. Xue, Y. Tian, X. Song, Z.-B. Liu, K. Xu, D. Zheng, F. Nori, and H. Fan, Simulating Chern insulators on a superconducting quantum processor, *Nat. Commun.* **14**, 5433 (2023).
- [61] S. E. Hamann, D. L. Haycock, G. Klose, P. H. Pax, I. H. Deutsch, and P. S. Jessen, Resolved-sideband Raman cooling to the ground state of an optical lattice, *Phys. Rev. Lett.* **80**, 4149 (1998).
- [62] A. M. Kaufman, B. J. Lester, and C. A. Regal, Cooling a single atom in an optical tweezer to its quantum ground state, *Phys. Rev. X* **2**, 041014 (2012).
- [63] E. Zohar, Y. Florshaim, O. Zilberman, A. Stern, and Y. Sagi, Degenerate Raman sideband cooling of ^{40}K atoms, *Phys. Rev. A* **106**, 063111 (2022).
- [64] J. T. Lü and J.-S. Wang, Coupled electron and phonon transport in one-dimensional atomic junctions, *Phys. Rev. B* **76**, 165418 (2007).
- [65] T. Brandes, Waiting times and noise in single particle transport, *Ann. Phys.* **520**, 477 (2008).
- [66] A. S. Mishchenko, N. Nagaosa, G. De Filippis, A. de Candia, and V. Cataudella, Mobility of Holstein polaron at finite temperature: An unbiased approach, *Phys. Rev. Lett.* **114**, 146401 (2015).
- [67] J. Li, D. Golez, G. Mazza, A. J. Millis, A. Georges, and M. Eckstein, Electromagnetic coupling in tight-binding models for strongly correlated light and matter, *Phys. Rev. B* **101**, 205140 (2020).
- [68] P.-C. Kuo, N. Lambert, M. Cirio, Y.-T. Huang, F. Nori, and Y.-N. Chen, Kondo QED: The Kondo effect and photon trapping in a two-impurity Anderson model ultrastrongly coupled to light, *Phys. Rev. Res.* **5**, 043177 (2023).
- [69] Y. Tanimura and S. Mukamel, Multistate quantum Fokker-Planck approach to nonadiabatic wave packet dynamics in pump-probe spectroscopy, *J. Chem. Phys.* **101**, 3049 (1994).
- [70] M. Cainelli and Y. Tanimura, Exciton transfer in organic photovoltaic cells: A role of local and nonlocal electron-phonon interactions in a donor domain, *J. Chem. Phys.* **154**, 034107 (2021).
- [71] S. Koyanagi and Y. Tanimura, Numerically “exact” simulations of a quantum Carnot cycle: Analysis using thermodynamic work diagrams, *J. Chem. Phys.* **157**, 084110 (2022).
- [72] M. Cirio, P.-C. Kuo, Y.-N. Chen, F. Nori, and N. Lambert, Canonical derivation of the fermionic influence superoperator, *Phys. Rev. B* **105**, 035121 (2022).
- [73] B. Debecker, J. Martin, and F. Damanet, Controlling matter phases beyond Markov, *Phys. Rev. Lett.* **133**, 140403 (2024).
- [74] J.-D. Lin, P.-C. Kuo, N. Lambert, A. Miranowicz, F. Nori, and Y.-N. Chen, Non-markovian quantum exceptional points, *Nat. Commun.* **16**, 1289 (2025).
- [75] T. Baumgratz, M. Cramer, and M. B. Plenio, Quantifying coherence, *Phys. Rev. Lett.* **113**, 140401 (2014).
- [76] A. M. Rey, L. Jiang, M. Fleischhauer, E. Demler, and M. D. Lukin, Many-body protected entanglement generation in interacting spin systems, *Phys. Rev. A* **77**, 052305 (2008).
- [77] A. Purkayastha, G. Guarnieri, M. T. Mitchison, R. Filip, and J. Goold, Tunable phonon-induced steady-state coherence in a double-quantum-dot charge qubit, *npj Quantum Inf.* **6**, 27 (2020).
- [78] G. Guarnieri, M. Kolář, and R. Filip, Steady-state coherences by composite system-bath interactions, *Phys. Rev. Lett.* **121**, 070401 (2018).
- [79] G. Ferioli, A. Glicenstein, F. Robicheaux, R. T. Sutherland, A. Browaeys, and I. Ferrier-Barbut, Laser-driven superradiant ensembles of two-level atoms near Dicke regime, *Phys. Rev. Lett.* **127**, 243602 (2021).
- [80] H. Jiang, L.-J. Lang, C. Yang, S.-L. Zhu, and S. Chen, Interplay of non-Hermitian skin effects and Anderson localization in nonreciprocal quasiperiodic lattices, *Phys. Rev. B* **100**, 054301 (2019).
- [81] S. Longhi, D. Gatti, and G. Della Valle, Robust light transport in non-Hermitian photonic lattices, *Sci. Rep.* **5**, 13376 (2015).
- [82] S. Weidemann, M. Kremer, T. Helbig, T. Hofmann, A. Stegmaier, M. Greiter, R. Thomale, and A. Szameit, Topological funneling of light, *Science* **368**, 311 (2020).
- [83] S. Mu, C. H. Lee, L. Li, and J. Gong, Emergent fermi surface in a many-body non-Hermitian fermionic chain, *Phys. Rev. B* **102**, 081115(R) (2020).
- [84] H. Geng, J. Y. Wei, M. H. Zou, L. Sheng, W. Chen, and D. Y. Xing, Nonreciprocal charge and spin transport induced by non-Hermitian skin effect in mesoscopic heterojunctions, *Phys. Rev. B* **107**, 035306 (2023).
- [85] S. Longhi, D. Gatti, and G. Della Valle, Non-Hermitian transparency and one-way transport in low-dimensional lattices by an imaginary gauge field, *Phys. Rev. B* **92**, 094204 (2015).
- [86] W. Gou, T. Chen, D. Xie, T. Xiao, T.-S. Deng, B. Gadway, W. Yi, and B. Yan, Tunable nonreciprocal quantum transport through a dissipative Aharonov-Bohm ring in ultracold atoms, *Phys. Rev. Lett.* **124**, 070402 (2020).
- [87] S. Mandal, R. Banerjee, E. A. Ostrovskaya, and T. C. H. Liew, Nonreciprocal transport of exciton polaritons in a non-Hermitian chain, *Phys. Rev. Lett.* **125**, 123902 (2020).
- [88] H. Ghaemi-Dizicheh and H. Schomerus, Compatibility of transport effects in non-Hermitian nonreciprocal systems, *Phys. Rev. A* **104**, 023515 (2021).
- [89] J. C. Budich and E. J. Bergholtz, Non-Hermitian topological sensors, *Phys. Rev. Lett.* **125**, 180403 (2020).
- [90] J. Wiersig, Enhancing the sensitivity of frequency and energy splitting detection by using exceptional points: Application to microcavity sensors for single-particle detection, *Phys. Rev. Lett.* **112**, 203901 (2014).